Review Article

Magnetism of Nanographene-Based Microporous Carbon and Its Applications: Interplay of Edge Geometry and Chemistry Details in the Edge State

Toshiaki Enoki[1,2,*] and Manabu Kiguchi[2]

[1]Toyota Physical and Chemical Research Institute, 41-1, Yokomichi, Nagakute, Aichi 480-1192, Japan
[2]Department of Chemistry, Tokyo Institute of Technology, 2-12-1 Ookayama, Meguro-ku, Tokyo 152-8551, Japan

(Received 31 July 2017; published 7 March 2018)

This paper is a contribution to the Physical Review Applied *collection in memory of Mildred S. Dresselhaus.*

Nanographenes have important edge geometry dependence in their electronic structures. In armchair edges, electron wave interference works to contribute to energetic stability. Meanwhile, zigzag edges possess an edge-localized and spin-polarized nonbonding edge state, which causes electronic, magnetic, and chemical activities. In addition to the geometry dependence, the electronic structures are seriously affected by edge chemistry details. The edge chemistry dependence together with edge geometries on the electronic structures are discussed with samples of randomly networked nanographenes (microporous activated carbon fibers) in pristine state and under high-temperature annealing. In the pristine sample with the edges oxidized in ambient atmospheric conditions, the edge state, which is otherwise unstable, can be stabilized because of the charge transfer from nanographene to terminating oxygen. Nanographene, whose edges consist of a combination of magnetic zigzag edges and nonmagnetic armchair edges, is found to be ferrimagnetic with a nonzero net magnetic moment created under the interplay between a strong intrazigzag-edge ferromagnetic interaction and intermediate-strength interzigzag-edge antiferromagnetic-ferromagnetic interaction. At heat-treatment temperatures just below the fusion start (approximately 1500 K), the edge-terminating structure is changed from oxygen-containing groups to hydrogen in the nanographene network. Additionally, hydrogen-terminated zigzag edges, which are present as the majority and chemically unstable, play a triggering role in fusion above 1500 K. The fusion start brings about an insulator-to-metal transition at $T_{I\text{-}M} \sim 1500$ K. Local fusions taking place percolatively between nanographenes work to expand the π-bond network, eventually resulting in the development of antiferromagnetic short-range order toward spin glass in the magnetic moments of nanographenes. For applications, the edge-state spins in nanographene-based microporous carbon can be a good tool as a molecule sensor in detecting molecules having different chemical properties and sizes. The on-off magnetic switching phenomena upon the adsorption of H_2O and other OH-containing molecules offers a molecule sensor. A He sensor, in which the edge-state spins is employed as a probe, is also proposed on the basis of a huge condensation of He into ultramicropores.

DOI: 10.1103/PhysRevApplied.9.037001

I. INTRODUCTION

Benzene is a hexagonal-shaped molecule consisting of sp^3 hybrid σ orbital and $2p_z$-based π orbital delocalized in the hexagon ring. Fusing benzene rings brings about polycyclic aromatic hydrocarbon molecules such as naphthalene, anthracene, and coronene, in which two, three, and seven rings are fused. Graphene is the extreme in the fusing process, in which an infinite number of rings are fused forming a two-dimensional (2D) hexagonal honeycomb lattice sheet. This is the chemistry bottom-up aspect, in which graphene is classified into polycyclic aromatic hydrocarbon molecules. We can discuss the electronic properties and chemical activities in terms of a phenomenological rule called Clar's aromatic sextet rule [1] for these molecules including infinite-size graphene. On the contrary, physicists discuss the same thing from the top-down aspect, in which small polycyclic aromatic hydrocarbon molecules are considered as fragments obtained by cutting an infinite graphene sheet. Here, the π conduction electrons described in terms of a massless Dirac fermion running in the 2D hexagonal bipartite lattice in graphene [2–4] are affected by the boundary condition of edges created by cutting into fragments. Accordingly, nanographenes, which are intermediate in size between infinite-size graphene and small polycyclic aromatic hydrocarbon molecules, are interesting nanomaterials which can be understood interestingly using both bottom-up chemistry language and top-down physics language [2–12].

According to the work of the present authors [5–7] and other groups [8–12], nanographenes have a wide variety of electronic, magnetic, and chemical properties depending

*tenoki@chem.titech.ac.jp

not only on their sizes and geometrical shapes but also on how the carbon atoms in the edges of nanographenes are terminated with various foreign chemical species. Therefore, a combination of chemical and physical aspects allows us to understand comprehensibly how the variety of electronic, magnetic, and chemical structures specific to nanographenes are created. Here, armchair and zigzag edges are fundamental edge geometries, and there is a clear contrast in the electronic structures between armchair and zigzag edges. In armchair edges, electron wave interference results in energetic stability, which gives a semiconducting electronic structure with an energy gap being opened [10,13]. This semiconducting electronic structure leads us to utilize armchair-edge nanographenes as nanocarbon-based field-effect transistors (FETs) [13,14]. The band gap, which is important in FETs, can be tuned by changing the ribbon width in graphene nanoribbons and/or edge chemical modifications [13]. In the meantime, a spin-polarized nonbonding edge state is created in the zigzag edges, which is the origin of electronic, magnetic, and chemical activities. Interestingly, the spins of the edge states form various magnetic structures such as ferromagnetic, antiferromagnetic, and ferrimagnetic structures in nanographenes depending on their edge shapes [15–19]. Consequently, zigzag-edged nanographene is expected to contribute to carbon-based magnetism and spintronic device applications [9,20,21]. In fact, zigzag-edged graphene nanoribbons with their edges being atomically precise have already been synthesized [9]. This means that the spintronic functions theoretically predicted can be reproduced with fidelity in practical applications.

Edge chemistry details add another set of variations to the electronic and magnetic structures that are modified primarily depending on the edge geometries [22–27]. The edge-chemistry-related variations offer chemical functionalities useful for applications such as chemical sensors, electrochemical devices, and catalysts as well [27]. In addition, the variations created by terminating-edge carbon atoms with oxygen-containing functional groups help us understand how to handle nanographenes and also graphitic or graphenic carbon materials for practical use in ambient atmospheric conditions. In fact, changing the functional group terminating edges from hydrogen to oxygen modifies seriously the electronic structure, as the latter having large electronegativity induces charge transfer from the graphene edge to the terminating oxygen. In this connection, tracking experimentally the variations by annealing nanographene sheets at high temperatures gives us important insight into edge chemistry. Pristine nanographenes prepared in ambient atmospheric conditions have edges terminated mostly with oxygen-containing functional groups. When nanographenes are annealed at high temperatures, heat-induced decompositions and the subsequent removal of functional groups take place, finally resulting in fusing nanographene sheets with each other in assembled nanographenes. Such a change in the chemistry details around the edges relies on the difference in the electronic structures of the functional groups whose energetic stabilities depend on the temperature of the heat treatment. Particularly, less stable zigzag edges are sensitive to the change in the edge chemistry related to the heat treatment. Fusing of nanographenes is triggered by the precursory formation of less stable edges in the temperature range just below where the fusion takes place.

In relation to a variety of graphene edges created under the combination of edge geometry and chemistry, intensive studies have been conducted using various graphitic materials, so far with a long-lasting important question to be answered on what the actual graphene edges are that are handled in the ambient atmosphere and/or under thermal history [28–34]. However, a conclusive answer remains to be given even though most of the graphitic materials practically utilized and the nanographene-based electronic devices, which are expected to be utilized in the future, are handled in ambient atmosphere and are oftentimes subjected to high-temperature treatments. Therefore, information on the edge geometry and chemistry details, which are linked tightly to the electronic, magnetic, or chemical properties of graphitic or graphenic materials, is indispensable in the development of graphite- or graphene-based technology.

In this article, we discuss the electronic and magnetic structures of nanographenes from the chemistry and physics aspects along with their edge geometry and chemistry dependence on the basis of the results of scanning tunneling microscopy or spectroscopy (STM or STS), electrical conductivity, magnetic susceptibility, ESR, near-edge x-ray absorption fine-structure spectroscopy (NEXAFS), temperature-programmed desorption (TPD), XPS, and first-principles calculations. We employ activated carbon fibers (ACFs) [35–40], which consist of a 3D disordered network of nanographene sheets (approximately 2–3 nm), except STM and STS observations in which the uppermost graphene layers of graphite with their edges monohydrogenated and carbonylated are used [7,41–43]. In relation to the correlation of the electronic and magnetic structures with the edge chemistry, we investigate the heat-treatment effect on the nanographene edges. The present systematic investigations of the chemical and physical characterizations with the employment of various experimental and theoretical tools give comprehensive and conclusive understanding of the question to be answered.

Edge-related functionalities, which are clarified from the above chemical and physical characterizations, are intriguing for device applications as well. Among these, the edge-state spins offer us a useful application in relation to the interplay of edge geometry and chemistry in the electronic or magnetic structures [44–46]. In this article, a molecule sensor and He detector, in which the edge-state spins are employed as a detection probe, are discussed

using nanographene-based microporous ACFs. Magnetic susceptibility and ESR investigations together with adsorption isotherm in ACFs inspire us to utilize a molecule-adsorption-induced change in the magnetic behavior of the edge-state spins for the sensor and detector.

II. ELECTRONIC STRUCTURES OF NANOGRAPHENES

Let us discuss the electronic structures of nanographene from the physics aspect [2–4]. The electrons running on the 2D hexagonal lattice of graphene can be described effectively in terms of a massless Dirac fermion as given by the Weyl equation, in which the kinetic energy has linear dependence on momentum $\mathbf{p}$ [2–4],

$$i\hbar\frac{\partial}{\partial t}\psi(r,t) = \begin{pmatrix} \hat{H}^* & 0 \\ 0 & \hat{H} \end{pmatrix}\psi(r,t),$$
$$\hat{H} = \sigma v_F \mathbf{p}, \tag{1}$$

where σ and v_F are the Pauli matrix and the Fermi velocity ($v_F = 3\gamma_0 a_{CC}/2\hbar$, $\gamma_0 = 3.16$ eV, intrasheet transfer integral and $a_{CC} = 0.142$ nm, intrasheet C—C bond length [47]), respectively. Here, the Pauli matrix σ is not associated with the real spin but with the pseudospin, which is effectively converted from the structural degree of freedom 2 in the 2D hexagonal bipartite lattice consisting of two independent sublattices as shown in Fig. 1(a) [2]. Namely, sublattices A and B are changed effectively to $\uparrow$, $\downarrow$ pseudospins. The electronic structure of graphene given by Eq. (1) is illustrated in Fig. 1(c) with the Dirac cones of the valence π and conduction $\pi*$ bands where the top of the former and the bottom of the latter touch each other at the Dirac point which is located at the Fermi level when graphene is neutral in charge, zero-gap semiconductor feature being suggested. Note that the structural degree of freedom 2 is conserved in the reciprocal lattice, and, consequently, we have two sets of Dirac cones at the K and K' points in the reciprocal space [Fig. 1(b)]. The presence of two valleys at the K and K' points related to the two sets of Dirac cones offers possible applications of graphene to valleytronics [48].

Chemistry can provide the same picture as that in physics, although the language is different. In chemistry, we can discuss the electronic structures and energetic stability of polycyclic aromatic hydrocarbon molecules and also graphene by tiling aromatic sextets on aromatic molecules or graphene. The aromatic sextet is a benzene ring in the resonance state with all six carbon atoms singly bonded to the surrounding atoms [Fig. 2(a)], According to Clar's rule [1], the most stable molecules or graphene fragments are those having the maximal number of sextets tiled. In the case of infinite graphene, the tiled sextets form a $\sqrt{3}\times\sqrt{3}$ superlattice, which is considered a kind of charge-density wave, as shown in Fig. 2(b). It should be noted here that Clar's representations are triply degenerate

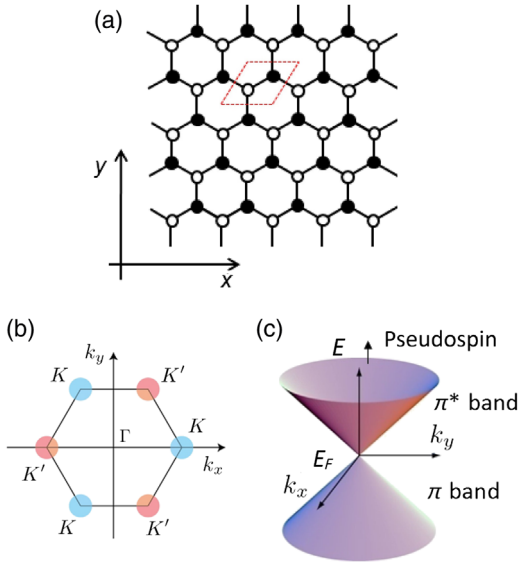

FIG. 1. (a) 2D hexagonal bipartite lattice of graphene with two independent sublattices (A, B), which are denoted with full and open circles, respectively. The dotted rhombus represents a unit cell. (b) The unit cell of the reciprocal lattice of graphene with two independent sublattice points K and K'. (c) Band structure of graphene with the Dirac cones of valence π and conduction π^* bands.

in infinite graphene owing to the presence of three independent hexagon rings in the graphene lattice. Therefore, the aromatic sextets migrate between the three states. This indicates that graphene is electrically conductive due to the delocalization of sextets, consistent with that predicted in physics.

We can discuss the electronic structures of nanographenes, which are considered nanofragments of graphene or nanosized polycyclic aromatic hydrocarbon molecules in physics or chemistry, respectively, in the same way. Here, the electronic structures depend on the geometry of open edges in addition to the size effect related to the quantum confinement. There are two fundamental directions—armchair and zigzag—when we cut a graphene sheet as exhibited in Fig. 3. By cutting a graphene sheet along these directions and subsequently terminating the edge carbon atoms with foreign chemical species such as hydrogen

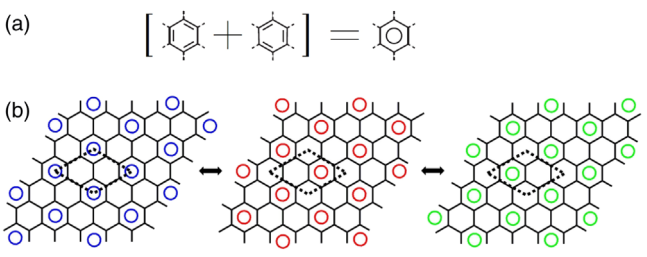

FIG. 2. (a) Aromatic sextet. (b) Infinite graphene shown with triply degenerate Clar's representations, in each of which a $\sqrt{3}\times\sqrt{3}$ superlattice (dotted rhombus) is formed.

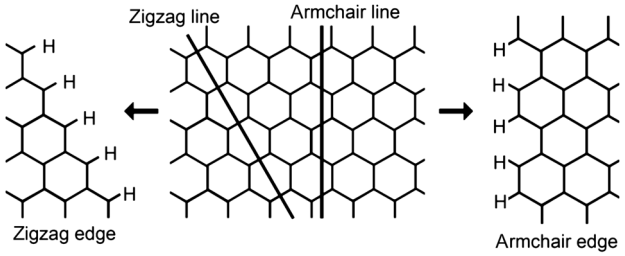

FIG. 3. Armchair and zigzag edges.

atoms, we can create two types of edge geometries, that is, armchair and zigzag edges. The created edges play the role of the boundary condition for the elastic scattering of the conduction π carriers having the feature of a massless Dirac fermion. The elastic scattering at an armchair edge changes the momentum from $\hbar k_x$ to $-\hbar k_x$ as shown in Fig. 4(a). This scattering corresponds to the transition from K to K' or K' to K in the reciprocal space [see Fig. 1(b)], that is, the intervalley transition. Accordingly, the scattered wave can be described in terms of a linear combination of wave functions at K and K',

$$\varphi_B(\mathbf{R}_B) \propto [-\exp(i\mathbf{K}\mathbf{R}_B) + \exp(i\mathbf{K}'\mathbf{R}_B)] \qquad (2)$$

for the carbon atom in sublattice B, and eventually electron wave interference is generated. In contrast, the scattering at a zigzag edge is given as transition $\hbar k_y \leftrightarrow -\hbar k_y$ [Fig. 4(b)], that is, the intravalley process within K or K' [see Fig. 1(b)]. Consequently, no interference takes place in a zigzag edge. The Weyl equation [Eq. (1)] indicates a difference between the armchair and zigzag edges in the perturbation by a magnetic field applied to nanographene or graphene edges. In magnetic field $\mathbf{B}$, the contribution from the gauge field $\mathbf{A}$ is added to the momentum $\mathbf{p} \to \mathbf{p} - e\mathbf{A}$, where $\mathbf{B} = \nabla \times \mathbf{A}$. Then, the Weyl equation is modified as

$$\hat{H} = \sigma v_F(\mathbf{p} - e\mathbf{A}). \qquad (3)$$

However, the magnetic field gives no substantial effect on an armchair edge, as the A or B symmetry is conserved; in other words, $\uparrow$ and $\downarrow$ pseudospins cancel each other, as can be seen in Fig. 4(c). In sharp contrast to the behavior of the armchair edge, a zigzag edge is affected by the magnetic field applied. Indeed, Fig. 4(d) shows the presence of only one of the sublattices (A, B) in a zigzag edge as a consequence of broken symmetry between sublattices A and B, and then the pseudospin behaves as real spin under the magnetic field applied. The spin-polarized state acting in the magnetic field in the vicinity of the zigzag edge is called the "edge state" [49–53].

The difference between the armchair and zigzag edges can be understood also in terms of the chemistry rule [6,7,11]. Figure 5 shows Clar's representations of armchair- and zigzag-edged molecules (fragments). Armchair-edged molecules have large numbers of sextets tiled [Fig. 5(a)],

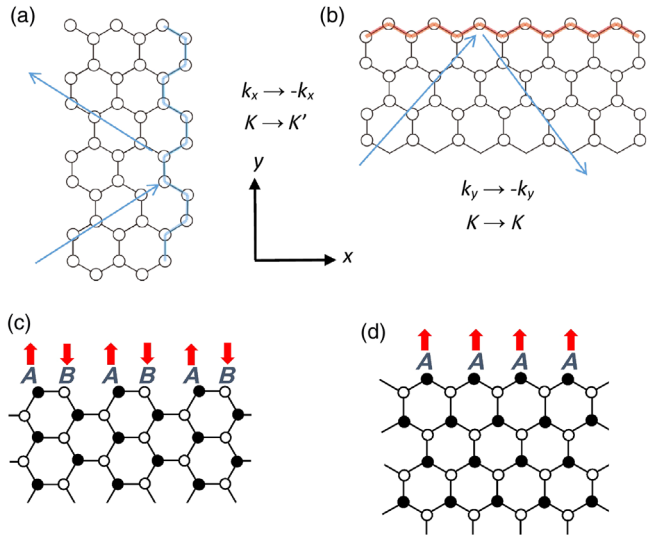

FIG. 4. Elastic scatterings at an armchair edge (a) and zigzag edge (b). The coordinate is given in the same way as in Fig. 1. Pseudospins in an armchair edge (c) and zigzag edge (d). The filled circle and open circle denote the A and B sublattices, respectively. The arrow denotes the pseudospins.

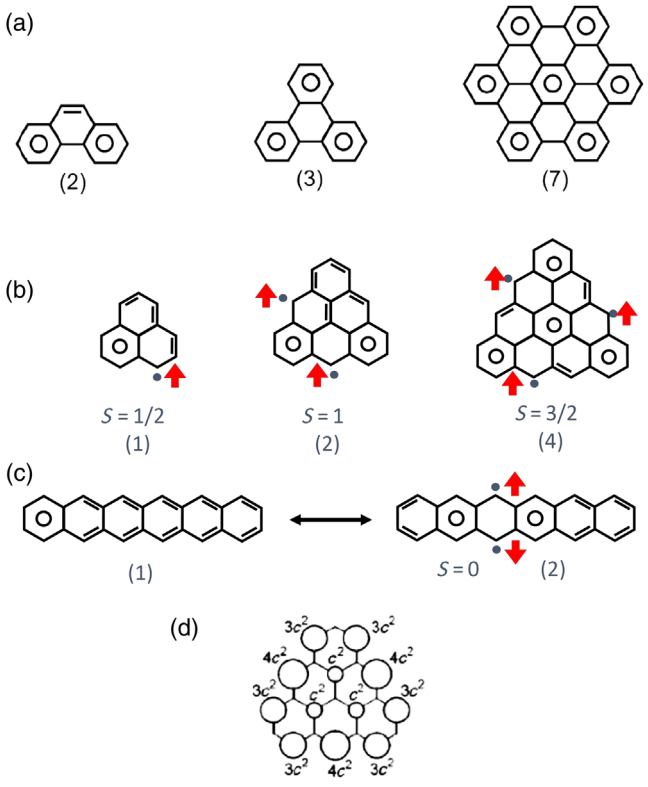

FIG. 5. The Clar's representations of (a) armchair-edged molecules, (b) zigzag-edged triangle molecules, and (c) zigzag-edged linear molecule. (d) Spatial distribution of the local density of states in the edge state of the triangle molecule consisting of six benzene rings. The number of sextets tiled is given in parentheses. The arrow with a dot denotes an unpaired electron with a spin of $s = 1/2$. The total spin is given with S.

being suggested to gain energetic (aromatic) stability. It should be noted that armchair-edged molecules have only one unique Clar's representation resulting in the localization of sextets, different from the migration of sextets in infinite graphene. The sextet localization indicates an insulating feature with an energy gap being open in armchair-edged molecules. This localization is due to the formation of a standing wave, which is understood to be associated with electron wave interference taking place in the armchair edges as discussed in physics before. The zigzag-edged molecules shown in Figs. 5(b) and 5(c) have small numbers of sextets, suggesting they are unstable. In addition, unpaired electrons, which occupy nonbonding π-electron states in single occupancy between bonding π and antibonding $\pi*$ states [Fig. 6(a)] remain in the part in which sextets cannot be tiled, consistent with what we discussed before in terms of the physics aspect of the edge state. The nonbonding states are localized in the vicinity of the zigzag edges as exhibited in Fig. 5(d), and accordingly, the edge state is named due to this edge localized feature [51–53]. The spins of unpaired electrons are arranged in parallel owing to the Hunt rule, forming a ferromagnetic state in the triangle molecules. In the case of the zigzag-edged linear molecules, the edge-state spins are arranged in an antiparallel or open-shell singlet state [54]. This suggests that the magnetic structures of the zigzag-edged molecules depend on their shapes. Another important feature, which differentiates the zigzag from the armchair, is the presence of multiple degeneracy, as shown in Fig. 6(b) for a zigzag-edged triangle molecule consisting of three benzene rings with 12 representations being degenerate. The migration of the sextets between 12 states, which confirms the absence of a standing wave together with the presence of the edge state (unpaired electron) suggests the unstable feature of zigzag-edged molecules again. The edge state having a large local density of states at the edges and a localized spin is responsible for the electronic, magnetic, and chemical activities in zigzag edges.

The variety of the electronic and magnetic structures depending on the edge geometry discussed in this section offers the important scientific basis for utilizing nanographenes in electronic and spintronic device applications.

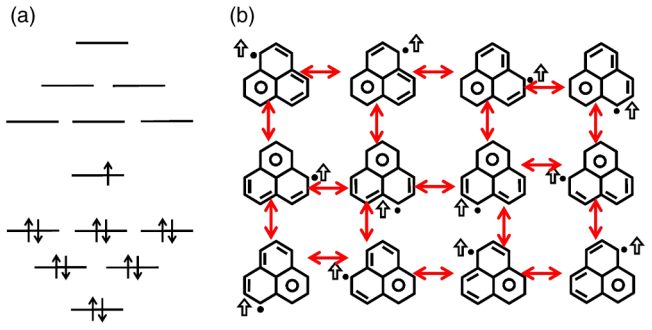

FIG. 6. The electronic structure (a) and 12 degenerate Clar's representations (b) of the zigzag-edged triangle molecule consisting of three benzene rings.

III. MAGNETIC STRUCTURE OF NANOGRAPHENE SHEETS RANDOMLY NETWORKED

We discuss the magnetic structure of nanographenes from experimental aspects on the basis of what is discussed theoretically in Sec. II, with the employment of nanographene-based ACFs as a model system. ACFs consist of a 3D disordered network of nanographene sheets having sizes of 2–3 nm [18,55–58], as shown in Fig. 7. Each nanographene sheet with its shape varying is made up of about 300 carbon atoms. Each sheet's periphery is formed with a combination of stable armchair and less stable zigzag edges, in the latter of which, the edge carbon atoms have electronically, magnetically, and chemically active nonbonding edge states. In each constituent nanographene, strong intra-zigzag-edge ferromagnetic exchange interaction J_0, whose strength is in the range of approximately 10^3 K, works to arrange edge-state spins ferromagnetically within a zigzag edge [59,60]. As shown in Fig. 7(b), ferromagnetically ordered zigzag edges, which are apart from each other with the presence of embedded nonmagnetic armchair edges, are weakly interacting with each other under the operation of inter-zigzag-edge exchange interaction J_1, whose strength is in the range of $J_1/J_0 \sim 10^{-1}$–10^{-2}. The strength and sign (ferromagnetic or antiferromagnetic) of J_1 vary depending on the distance

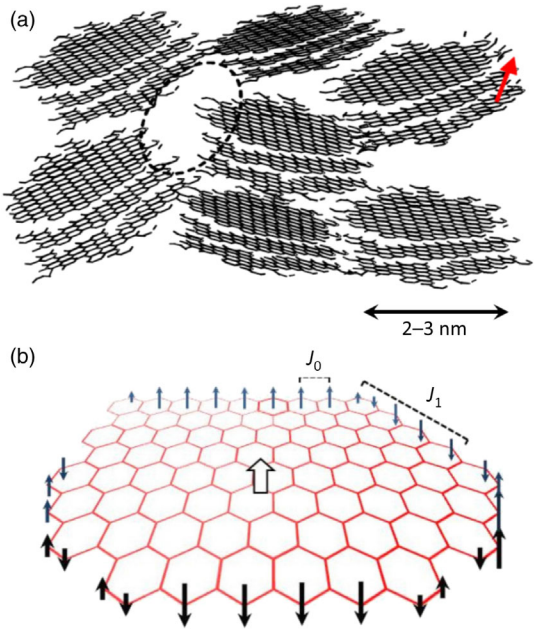

FIG. 7. (a) Schematic of the ACFs consisting of a 3D disordered network of nanographene sheets. The arrow represents a magnetic moment associated with edge-state spins. The dashed circle denotes a nanopore surrounded by nanographene sheets. (b) Nanographene sheet in ACFs. The arrow represents an edge-state spin (↑,↓). J_0 and J_1 denote intra-zigzag-edge ferromagnetic interaction and inter-zigzag-edge ferromagnetic or antiferromagnetic interaction, respectively. The open arrow represents a net magnetic moment created under the cooperation of J_0 and J_1.

and mutual geometrical relation between the zigzag edges concerned [59]. Accordingly, the cooperation of strong ferromagnetic J_0 and intermediate-strength ferromagnetic or antiferromagnetic J_1 is predicted to give a ferrimagnetic (superparamagnetic) structure with a nonzero net magnetic moment in an individual arbitrarily shaped nanographene sheet after the compensation of magnetic moments between ferromagnetic zigzag edges [Fig. 7(b)] [37]. The magnetic and electronic behavior predicted above can be tracked experimentally using magnetic susceptibility, ESR, and electrical conductivities as shown in Fig. 8[37].

The static magnetic susceptibility χ shown in Fig. 8(c) obeys the Curie-Weiss law in the entire temperature range down to 2 K with a weak negative Weiss temperature of

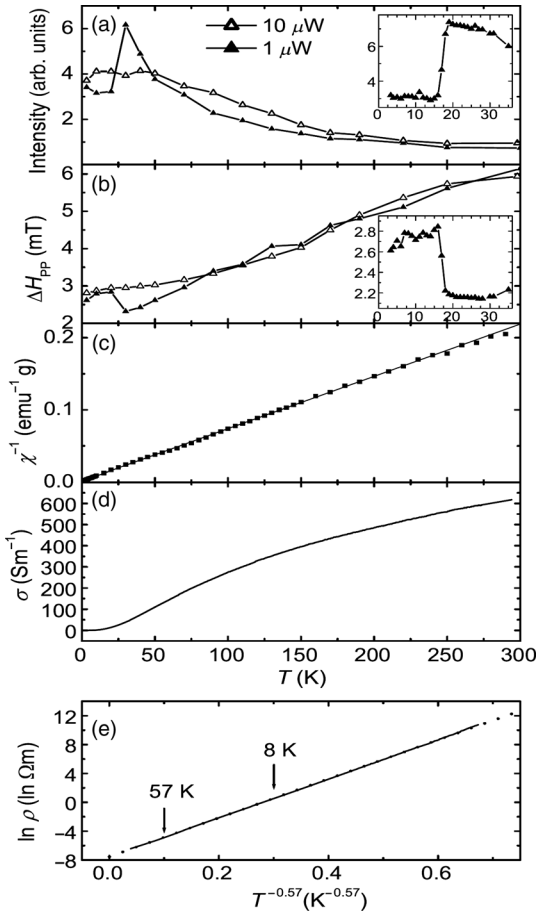

FIG. 8. The magnetic and electron-transport properties of the pristine ACFs. (a) Temperature dependence of the ESR intensity in vacuum at 1-μW (filled triangle) and 10-μW (open triangle) microwave powers. (b) The corresponding peak-to-peak widths of the ESR signal obtained after fitting the Lorentzian function. Inset of (a) and (b): Enlarged curves in the range of 4–35 K for 1 μW. (c) Inverse static susceptibility as a function of the temperature in vacuum (square) and the linear fit (solid line). (d) Temperature dependence of the dc conductivity in vacuum. (e) Conductivity vs temperature plot corresponding to (d) and linear fit (dotted line). The arrows correspond to 57 and 8 K. (After Ref. [37].)

$\Theta \sim -2$–3 K, indicating that the magnetic moments of the nanographene sheets are interacting weakly with each other under the operation of weak antiferromagnetic inter-nanographene-sheet interaction J_2. The magnetic moment from Curie's constant is estimated as approximately 10^{-3} μ_B/C, which is in good quantitative agreement with that expected from Clar's rule for a nanographene sheet having approximately 300 carbon atoms. However, the ESR spectra show a different face in the behavior of the magnetic moments of nanographene sheets as evidenced in Figs. 8(a) and 8(b) for the intensity and linewidth, respectively. Indeed, the ESR intensity, which corresponds to the dynamical susceptibility, indicates a sharp drop below approximately 20 K, at which the intensity is peaked, for a microwave power of 1 μW, although it obeys Curie's law above the temperature of the peak, consistent with the static susceptibility. In an elevated microwave power of 10 μW, the sharp discontinuity observed in 1 μW fades away, resulting in the appearance of a broad hump around the peak temperature of approximately 20 K. In addition, the ESR linewidth ΔH_{PP} for a microwave power of 1 μW has an abrupt discontinuity at the temperature of the intensity peak. ΔH_{PP} is linearly dependent on the temperature above 20 K, while it exhibits a discontinuous upsurge below the temperature of the intensity peak. ΔH_{PP} becomes smooth in the entire temperature range for 10 μW. The ESR spectral profiles give us more information on the dynamical behavior of the magnetic moments of nanographenes. Above the temperature of the intensity peak, the line shape has a feature of Lorentzian together with the absence of microwave power saturation, suggesting that the spin system of the disordered network of nanographene sheets in ACFs is homogeneous because of the motional or exchange narrowing effect. In contrast, below that temperature, the ESR line shape deviates from Lorentzian, and the intensity becomes easily saturated in elevated microwave powers. Interestingly, the ESR signal shows an irregular shape related to a hole-burning phenomenon [61] under an intense microwave power of 16 mW in the vicinity of the discontinuous change in the ESR linewidth [37]. The appearance of the hole-burning phenomenon gives important evidence for the presence of a static distribution of ESR on-resonance fields, for which the structural inhomogeneity in the disorderedly networked nanographene is responsible. These findings on the ESR line profiles importantly proves that the spin system becomes inhomogeneous below 20 K. In this connection, the electrical conductivity gives a clue for understanding what is happening with the behavior of the magnetic moments of nanographenes. Figures 8(d) and 8(e) show the temperature dependence of the conductivity. The conductivity, which is lowered with the lowering of the temperature, obeys the Coulomb-gap-type variable range-hopping mechanism given by the following equation [35,62,63]:

$$\sigma(T) = \sigma_0 \exp[-(T_0/T)^{\gamma}], \qquad \gamma = 1/2. \tag{4}$$

Eventually, the electron transport is governed by the hopping process of conduction electrons between nanographene sheets in the random nanographene network under the influence of Coulomb interaction, and at low temperatures, the conduction carriers become localized within individual nanographene sheets. We should remind that the deviation in the experimentally observed γ (=0.57) from $\gamma = 1/2$ proves a fractal feature in the random network [64,65]. With this conductivity behavior, the inhomogeneity in the dynamical behavior of the magnetic moments of nanographenes can be understood on the basis of the carrier localization taking place at low temperatures. In the high-temperature range, the mobile electrons in the transport between nanographene sheets make the magnetic moments of nanographenes subject to motional narrowing, bringing about the homogeneous feature in the spin system with the Lorentzian-shaped ESR signal. The ESR linewidth, which is proportional to the temperature in the high-temperature range, is associated with the Korringa-type spin-lattice relaxation process mediated by the conduction carriers [66,67], suggesting the important role of mobile electrons. This Korringa-type relaxation is consistent with the behavior of electron transport. The strong coupling between the edge-state spins and conduction carriers along with the weak spin-orbit interaction of graphene (5 cm^{-1} [68]) leads to a bottleneck in energy dissipation from the conduction carriers to the lattice. This energy dissipation gives the inverse proportionality of the spin-lattice relaxation time $T_{1\mathrm{eff}}$ ($\propto 1/\Delta H_{\mathrm{PP}}$) with the temperature as observed. The localization of carriers that mediate internanographene interaction makes constituent nanographene sheets independent of each other at low temperatures below 20 K. Each nanographene sheet has its own strength of the magnetic moment, depending on its size and shape. Consequently, the on-resonance magnetic fields in the ESR signal distribute randomly depending on the constituent nanographene sheets having various sizes and shapes. Eventually, the spin system becomes inhomogeneous as observed at low temperatures, at which motional narrowing is not at work due to the carrier localization. These findings confirm that an individual nanographene sheet behaves ferrimagnetically (superparamagnetic in other words) with a nonzero net magnetic moment, whose strength depends on its size and shape.

The magnetic structures varying in a wide range from ferromagnetic, antiferromagnetic to ferrimagnetic allow us to take nanographenes as an important constituent to molecular-based magnetism and its applications [69].

IV. ELECTRONIC AND MAGNETIC STRUCTURES OF EDGE STATES AFFECTED BY THE CHANGE IN CHEMICAL ENVIRONMENTS UNDER HIGH-TEMPERATURE ANNEALING

The edges of the nanographene samples handled in ambient atmospheric condition are oxidized, resulting in edge carbon atoms terminated mostly with oxygen-containing functional groups [30,32,70,71]. When they are annealed in vacuum under elevated temperatures, the oxygen-containing functional groups existing in the atmospheric condition become decomposed and removed successively. Finally, above 1500 K, nanographenes fuse with each other in an assembly of nanographene sheets, and eventually, larger nanographene sheets grow [35,36]. Note that annealing in the oxygen atmosphere at high temperatures results in oxidizing unstable zigzag edges preferentially, and the fraction of armchair edges increases accordingly as zigzag edges are etched out [71]. Here, we discuss how the electronic and magnetic structures are modified under the change in the edge chemistry toward the fusion of nanographene sheets in high-temperature annealing in vacuum with spin-polarized nonbonding edge states as an important monitor. In the experiment, we employ microporous ACFs (Fig. 7), which are discussed in Sec. III. Note that the information in this section on the air sensitivity and stability and thermal history effect on the edge chemistry and the electronic or magnetic structures of nanographenes is indispensable in not only understanding what actual graphene edges are [28–32] but also in utilizing nanographenes for device applications [13,14,20].

Figure 9 shows the changes in the chemical environment of nanographene edges with experimental results of TPD and O 1s XPS spectra [40]. As evidenced in Figs. 9(a) and 9(b) for the TPD spectra and their integrated values, respectively, in the temperature range up to 2100 K, the desorbed H_2O, CO_2, CO, and H_2 species in the mass spectra have TPD peaks appearing at 400–1200 K (600 K), 400–1000 K (600 K), 400–1500 K (1200 K), and 1100–2000 K (1400 K), where the value in parentheses is the position of the observed peak. This finding indicates the temperature-dependent decomposition process of functional groups terminating the edge carbon atoms. Figure 9(c) for the O 1s XPS proves that the two types of oxygen-containing functional groups −OH and >C=O are present in the temperature range of 900–1400 K. The experimental results prove that the decompositions of the functional groups take place as follows: −COOH at approximately 600 K, −OH and >C=O at 1200 K, and finally, −H at 1500 K. Above 1800 K, the edges become completely naked. Taking into account that the fusion of nanographenes starts at around 1500 K [35], it is suggested that the fusion is subjected to the removal process of hydrogen atoms from the edge carbon atoms, as only hydrogen atoms remain bonded to the edge carbon atoms in the temperature range in which the fusion takes place.

Here we should answer the following two questions in relation to the chemical changes and fusion, in which chemically active zigzag edges play an important role as a front in the chemical reactions [71]. How can the edge state, which is usually unstable, survive in zigzag edges handled in ambient atmosphere? Why does the fusion take place in a condition where hydrogen-terminated edges are abundant in the temperature regime just below where the fusion

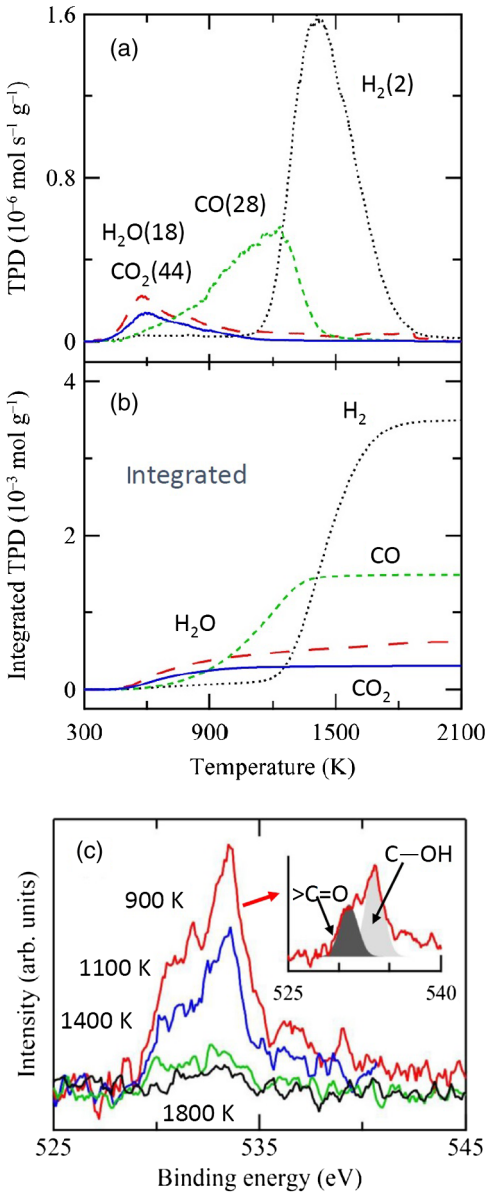

FIG. 9. (a) The TPD spectra, (b) integrated TPD spectra, and (c) O 1*s* XPS of ACFs depending on the heat-treatment temperature in vacuum. In the inset of (c), the spectrum of 900 K is deconvoluted into two Gaussians assigned to >C=O and C—OH. (After Ref. [40].)

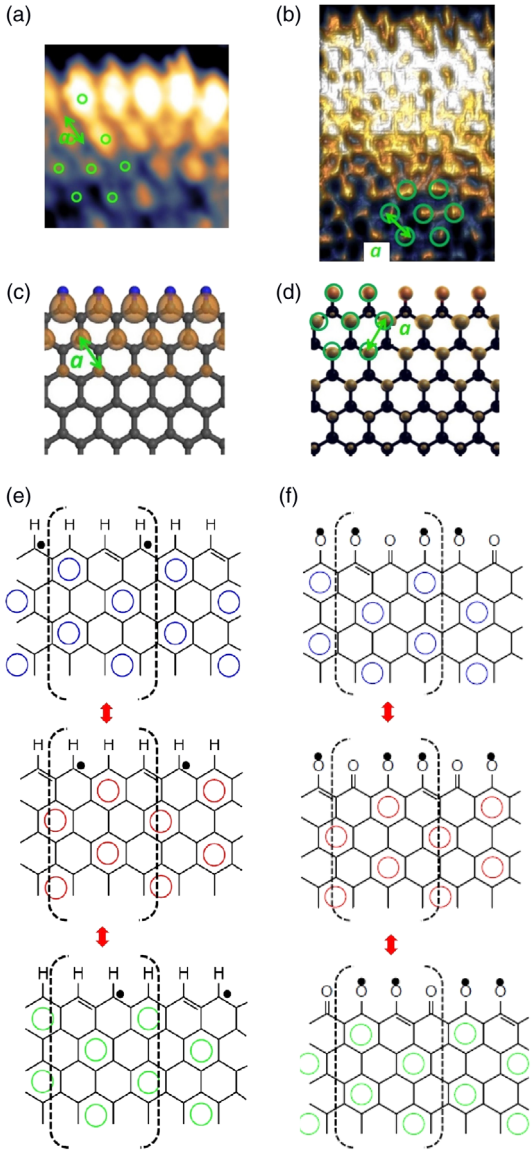

FIG. 10. The STM images, spatial distributions of the local density of states for the edge states obtained by DTF calculations, and Clar's representations in the vicinity of zigzag edges monohydrogenated (a),(c),(e) and carbonylated (b),(d),(f). The bright spots in the STM images (a) and (b) are assigned to the edge state. The green circles with an arrow denote the unit cell with the lattice constant $a = 0.246$ nm. The Clar's representations are triply degenerate in (e) and (f). The filled dot denotes an unpaired electron. (After Ref. [7].)

starts? To answer these questions, Fig. 10 shows a comparison of the edge states between a zigzag edge bonded with an oxygen-containing functional group (carbonyl > C=O) and that with hydrogen, with the results of STM observations, density-functional theory calculations, and Clar's representations [7,41,42]. In the case of a zigzag edge terminated with a carbonyl group, the hybridization of the π orbital in the carbon atoms and the $2p_z$ orbital in the terminating oxygen atoms, both of which are aligned perpendicular to the graphene sheet, is formed, resulting in charge transfer from nanographene to electronegative oxygen atoms. This charge transfer makes the edge state possess less localized features. Indeed, the local density of states of the edge state is extended to the terminating oxygen atoms and also to the interior of the nanographene sheet with an elongated decay length (approximately 2 nm) of the wave function of the edge state, as confirmed by the observed STM atomic image and calculated spatial distribution of the local density of states for the edge state [Figs. 10(b) and 10(d), respectively]. The less localized feature of the active edge state, which is

shared by the terminating oxygen atoms and carbon atoms from the edge to the interior of a nanographene sheet, allows the edge state to be stabilized even in the ambient atmospheric condition, as we can see in the last section and later. In sharp contrast, the hydrogen-terminated zigzag edge has an edge state well localized in the vicinity of edges, as shown in Figs. 10(a) and 10(c), and accordingly, a large concentration of active unpaired electrons condensed in the edge carbon atoms makes the edges unstable. This unstable structure is favorable for fusing nanographene sheets at high temperatures. The presence of easily removable hydrogen atoms present in the edge region facilitates the fusion process between nanographene sheets facing each other upon the removal of the hydrogen atoms as the precursor of fusion.

Next, we discuss what happens in the electronic and magnetic structures of nanographenes and their random network in relation to the change in the edge chemistry under heat treatment at high temperatures. Figure 11 exhibits the C K-edge NEXAFS spectra as a function of heat-treatment temperature up to 1800 K in vacuum for ACFs [40]. The peaks at 293 and 285.5 eV are assigned to the σ^* and π^* bands, respectively, confirming the sample to

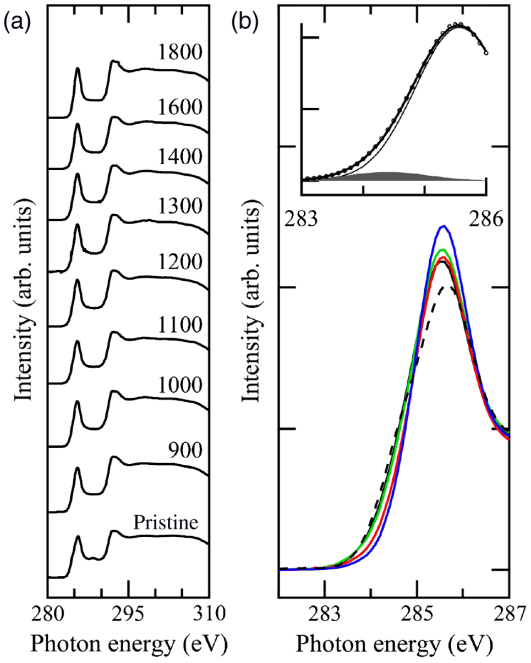

FIG. 11. (a) The C K-edge NEXAFS spectra of the ACFs after heat treatments at various heat-treatment temperatures. (b) The close-up of the preedge region of the C K-edge NEXAFS spectra of the ACFs heated at 900 K (black curve), 1400 K (green curve), 1600 K (red curve), and 1800 K (blue curve). The dotted line is the NEXAFS spectra of the pristine ACFs. The inset shows the spectrum of the sample heated at 900 K (circles) and double Gaussian fits (thin line and dark gray region assigned to the π^* conduction band and the edge state, respectively). The sum of the two Gaussian peaks is denoted by the solid curve. (After Ref. [40].)

be graphitic (graphenic). The finding that the spectral features are well preserved up to the highest temperature in the experiment suggests the stability of the graphenic structure. Importantly, we notice the presence of a small peak 284.5 eV just below the π^*-conduction band, as seen in deconvoluting the observed spectrum in terms of two Gaussians [Fig. 11(b)]. This proves the presence of a nonbonding state assigned to the edge state in the vicinity of the Fermi level just below the π^*-conduction band [38,39,72]. Note that the observed chemical shift $\Delta = -1.0$ eV (= 284.5–285.5 eV), the absolute value of which is considerably larger than that of the σ-dangling bond [$\Delta = -0.6$ eV (=284.9–285.5 eV)] proves a large screening effect of the π electrons acting on the nonbonding state. This large screening effect allows us to assign the observed nonbonding state to the edge state of π origin. The edge state fades away upon the elevation of the heat-treatment temperature from 900 up to 1600 K, accompanied by the sharpening of the π^*-conduction band [Fig. 11(b)].

Figure 12 summarizes the heat-treatment temperature-dependent variations of the TPD and NEXAFS spectra together with the accompanying changes in the electrical resistivity and the magnetic susceptibility. The changes in the oxygen-to-carbon (O:C) atomic ratio and the hydrogen concentration (n_H) shown in Figs. 12(a) and 12(e), respectively, are considered to be related to the change in functional groups bonded to the edges of individual nanographene sheets, since the pristine ACFs have well-graphitized structures, and only the edge regions are affected by the high-temperature annealing with the interior of nanographene remaining intact as evidenced in the NEXAFS spectra (Fig. 11) [40]. The O:C atomic ratio declines monotonically upon the elevation of the heat-treatment temperature up to 1500 K, and it becomes independent of the heat-treatment temperature above that temperature. Meanwhile, the hydrogen concentration (n_H) has only weak heat-treatment temperature dependence in the low-heat-treatment temperature regime, and it gets a steep decrease above 1300 K. Finally, the change becomes moderate above 1500 K, which corresponds to the temperature at which the fusion of nanographene starts. As n_H remains finite and shows a gradual decrease up to 1800 K, the fusion is suggested to proceed at the expense of terminating hydrogen atoms.

The changes in the edge chemistry details seriously affect the electronic and magnetic structure of nanographenes. The electrical resistance (measured by the two-probe method), which internanographene electron transport governs, decreases monotonically as the heat-treatment temperature is elevated to the temperature of the fusion start (approximately 1500 K), and then it becomes less heat-treatment temperature dependent above that temperature. The detailed variation in the electron transport dependent on the heat-treatment temperature is shown in Fig. 13(a). The electrical conductivity (measured by the four-probe method)

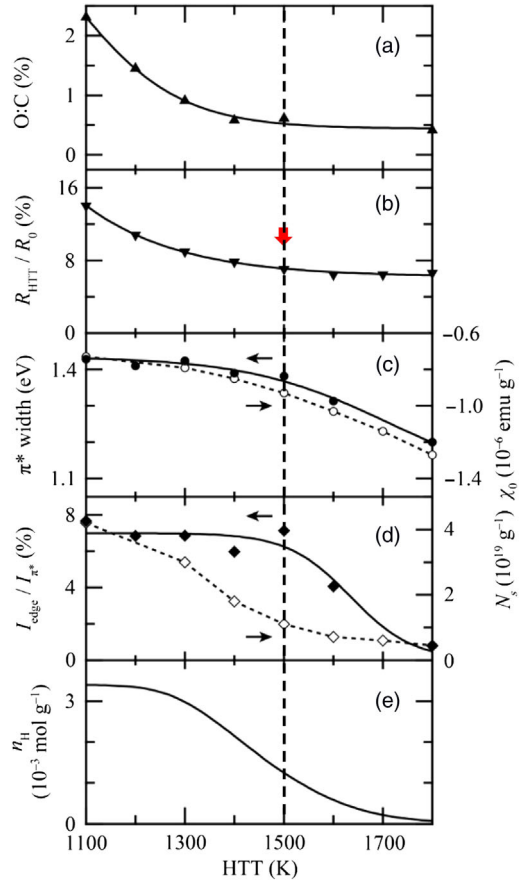

FIG. 12. Heat-treatment temperature (HTT) dependence of (a) the O:C ratio, (b) the electrical resistance (R_{HTT}/R_0) (R_0 is the resistance before high-temperature heat treatment), (c) the π^*-band width in NEXAFS (solid line) and the diamagnetic susceptibility (χ_0) (dashed line), (d) the spectral intensity of the edge state in NEXAFS ($I_{edge}/I_{\pi*}$) (relative to the π^*-band intensity) (solid line) and the spin concentration of the edge state (N_s) (dashed line), and (e) the hydrogen concentration (n_H) in the ACFs. The vertical dashed line denotes the temperature at which an insulator-to-metal transition takes place. Two-probe method is employed in the electrical resistance measurement. (After Ref. [40].)

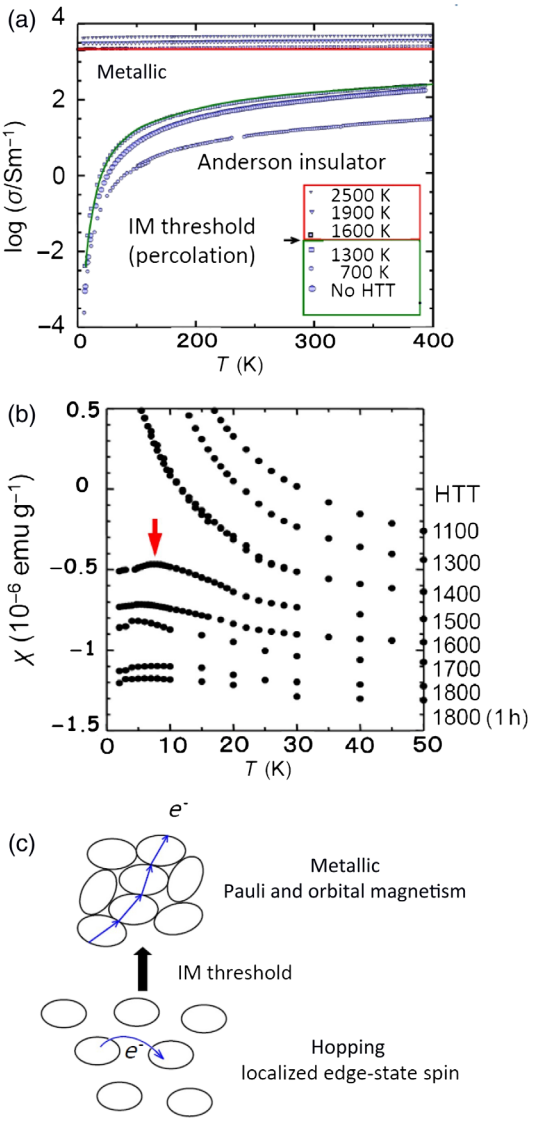

FIG. 13. Temperature dependence of the electrical conductivity (σ) (a) and the magnetic susceptibility (χ) (b) of the ACFs in heat treatment at different HTTs. The heat-treatment time in (b) is 15 min except for 1800 (1 h) in which the sample is treated for 1 h. (c) Schematic for the change in the electron transport and magnetic structures in the vicinity of the *I*-*M* transition. (After Refs. [35,36].)

behaves insulating in the low heat-treatment temperature range below 1300 K, confirming again the results shown in Figs. 8(d) and 8(e), in which the internanographene electron transport can be explained in terms of the Coulomb-gap-type variable-range-hopping process in the random nanographene network in the Anderson insulator, in which serious randomness brings about electron localization at low temperatures [Fig. 13(c)]. This insulating behavior remains unchanged up to the temperature the of fusion start. At the temperature of the fusion start, the conductivity shows a discontinuous upsurge, and above that temperature, metallic behavior appears in the conductivity, despite less temperature dependence owing to the effect of serious randomness in the nanographene network. The disordered metal behavior appearing above 1500 K suggests the onset of an insulator-to-metal transition at that temperature, above which coherent electron-transport paths are created in the entire nanographene network [Fig. 13(c)]. Consequently, the temperature of the fusion start matches the temperature of the insulator-to-metal transition ($T_{I\text{-}M}$). This can be understood in terms of the percolation threshold of coherent electron-transport paths, above which all of the constituent nanographene sheets become connected to each other with the aid of the coherent electron-transport paths in the entire nanographene network. In other words, in the vicinity of the temperature of the fusion start, local fusions develop percolatively, and all of the nanographene sheets are bonded to each other with $sp^3 + \pi$ bonds created at their

edges above the temperature of the fusion start, forming the metallic electronic structure.

Let us examine the heat-treatment temperature dependence of the electronic structure of the π electrons in terms of the π^*-band width in the NEXAFS spectra and the diamagnetic susceptibility χ_0, both of which represent the extension of the π^*-electron network shown in Fig. 12(c). These two physical quantities have almost the same trend in heat-treatment temperature dependence, and both tend to decrease above around the temperature of the fusion start. This suggests that the size of the nanographene becomes larger successively as the result of the fusion of nanographene sheets above that temperature, consistent with the experimental results of the electrical conductivity. Here is an important question to be answered about what happens in the edge states which are present in the vicinity of the zigzag edges of nanographene sheets. The edge-state contribution ($I_{\rm edge}$), which is proportional to the number of edge states, in the NEXAFS spectra shown in Fig. 12(d) has no change in the temperature range just below the temperature of the fusion start, suggesting that the number and sizes of the nanographene sheets remain unchanged and that the number of edge states is insensitive to the change in chemical species bonded to the edge carbon atoms though the electronic feature of the edge states varies depending on how the edge carbon atoms are bonded to the foreign chemical species. In other words, we can confirm experimentally the theoretical prediction that the number of edge states depends on the size and geometry of the nanographene sheet. When the heat-treatment temperature exceeds the temperature of the fusion start, $I_{\rm edge}$ shows a steep decrease, importantly suggesting that fusing works to reduce the number of edge states due to the disappearance of the edges.

The magnetic susceptibility of the edge state allows us to gain insight into what happens in the edge-state spins [35,36]. Figure 13(b) shows the temperature dependence of the static magnetic susceptibility χ. In the Anderson insulator regime below $T_{I\text{-}M}$, χ obeys the Curie-Weiss law with a small negative Weiss temperature of $\Theta \sim -2$–3 K, suggesting that the ferrimagnetic moments of the nanographene sheets are interacting with each other under the operation of weak antiferromagnetic internanographene interaction J_2, similar to that in non-heat-treated pristine ACFs [Fig. 8(c)]. Above $T_{I\text{-}M}$, the magnetic susceptibility loses the localized spin nature, and instead, less temperature-dependent negative susceptibility indicates the coexistence of a small positive Pauli paramagnetic conduction carrier contribution and a large negative orbital contribution. Eventually, the formation of a metallic state is suggested again in the disordered nanographene network above $T_{I\text{-}M}$, in good agreement with the behavior of electrical conductivity [Fig. 13(a)]. Here it should be noted that an anomalous feature appears in the vicinity of the I-M transition; that is, a small hump is observed around 7 K in the susceptibility. It looks like a hump related to the onset of antiferromagnetic ordering, but this is not the case in the present result, as we have a clear magnetic-field-cooling effect in the behavior of the magnetic susceptibility in the vicinity of $T_{I\text{-}M} = 1500$ K, even though the field-cooling effect is absent in the sample heat treated well below $T_{I\text{-}M} = 1500$ K, as exhibited in Fig. 14. The large field-cooling effect is evidence of the formation of a spin-glass-like state in the random nanographene network in which the ferrimagnetic magnetic moments of nanographene sheets with their strengths depending on their shape and sizes are frozen in a random fashion [35,36]. Actually, the deviation of the effective exchange interactions observed in the magnetization curve is estimated as $\sqrt{\langle \Delta J \rangle^2 / \langle J \rangle} \sim 0.8$. The large randomness in the exchange interaction is responsible for the formation of the spin-glass-like state in the vicinity of the I-M transition.

Finally, we discuss the heat-treatment temperature dependence of the internanographene exchange interaction J_2. Figure 12(d) shows the comparison between the spectral intensity of the edge state in NEXAFS ($I_{\rm edge}/I_{\pi *}$) and the spin concentration of the edge state (N_s). If there is no interaction between the magnetic moments of the nanographene sheets, then both should have the same trend in the heat-treatment temperature dependence. However, there is a large difference between the two quantities, particularly in the heat-treatment temperature range around the I-M transition. As a matter of fact, the edge-state spin concentration decreases faster than the number of edge states (represented by $I_{\rm edge}/I_{\pi *}$), suggesting the development of antiferromagnetic short-range ordering as we approach the I-M transition temperature. This finding importantly proves the indispensable role of the internanographene exchange interaction J_2 in magnetic behavior. Figure 15 shows the ratio of $N_s/I_{\rm edge}$ as a function of heat-treatment temperature and the effective exchange interaction acting

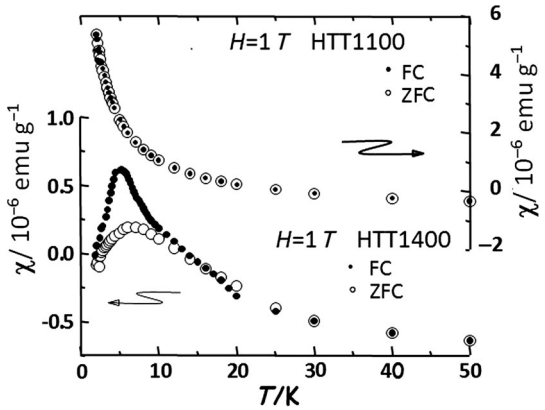

FIG. 14. Magnetic-field-cooling effect on the magnetic susceptibility of the ACFs heat treated in the vicinity of and well below the insulator-to-metal transition temperature shown as HTT1400 and HTT1100, respectively. FC and ZFC denote field cooling at $H = 1$ T and zero-field cooling, respectively. (After Ref. [36].)

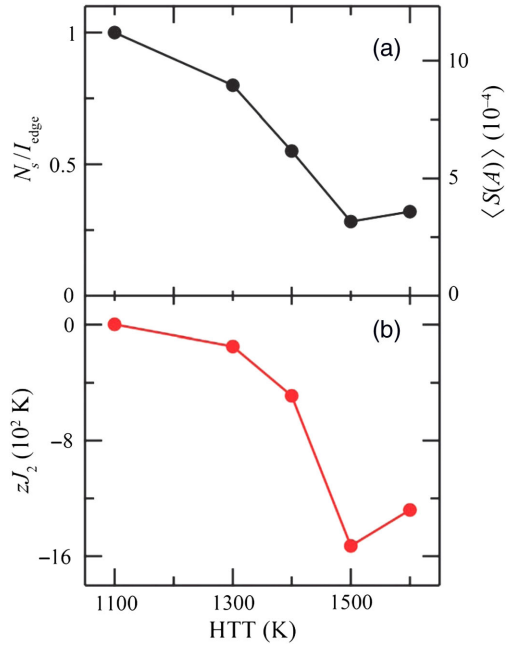

FIG. 15. (a) Heat-treatment temperature dependence of the ratio of the edge-state spin concentration to the spectral intensity of the edge state in the NEXAFS spectra (N_s/I_{edge}) and the thermal average of edge-state spin $\langle S(A)\rangle$ under the internal magnetic field A. The value of N_s/I_{edge} is normalized with respect to the value at HTT = 1100 K. (b) The internal magnetic field (zJ_2) acting between the magnetic moments of nanographene sheets. (After Ref. [40].)

between the magnetic moments of edge-state spins between the nanographene sheets. A decrease in the ratio of N_s/I_{edge} is suggestive of the antiferromagnetic interaction between the nanographene sheets growing upon heat treatment, and we estimate the effective exchange interaction using a simple mean-field treatment as given in the following equation:

$$\begin{aligned}&\langle S\rangle \propto N_S/I_{edge},\\ &\langle S\rangle = \frac{M(A)}{N_{edge}g\mu_B} = SB_S\left(\frac{g\mu_B S(H+A\langle S\rangle)}{k_BT}\right),\\ &A = \frac{2zJ_2}{g\mu_B}.\end{aligned} \tag{5}$$

Here, we assume that the thermal average of spin $\langle S\rangle$ is proportional to the ratio of N_s/I_{edge} and given by the Brillouin function $B_S(x)$ under the influence of internal magnetic field (A, molecular field coefficient). The internal field is simply assumed to come from the internanographene exchange interaction J_2 with the number of nearest neighbors being z, though the assumption is too simplified. However, this simplified analysis can offer important information on what happens in the interaction between the ferrimagnetic moments in the vicinity of the I-M transition. Equation (5) gives the heat-treatment temperature dependence of the effective exchange interaction as shown in Fig. 15(b). In the heat-treatment temperature regime well below the temperature of the fusion start, the exchange interaction zJ_2 is small and antiferromagnetic as we have already discussed. The absolute value of zJ_2 increases steeply as we approach the I-M transition, and it becomes approximately 10^3 K, which is almost similar to the strength of the intrananographene interaction. This suggests that the magnetic moment of edge-state spins in a nanographene sheet interacts strongly with that of an adjacent nanographene sheet through a strong antiferromagnetic interaction J_2, for which covalent π-bonding bridges formed by local fusion between the nanographene sheets are responsible, in the vicinity of the temperature of the fusion start. As a consequence, antiferromagnetic short-range order develops in the magnetic moments of networked nanographene sheets, resulting in the formation of the spin-glass state at the I-M transition.

V. APPLICATIONS OF THE EDGE-STATE SPINS AS A PROBE OF MOLECULE SENSORS IN MICROPOROUS ACTIVATED CARBON

Microporous ACFs, which consist of a 3D disordered network of nanographite domains as explained schematically in Ref. [55] Fig. 7, have huge specific surface areas of approximately 3000 m^2/g in their micropores [73,74]. Here, each nanographite domain is comprised of a loose stack of three to four nanographene sheets (2–3 nm in size) with an internanographene sheet distance of 0.38 nm [75], which is considerably elongated in comparison with the interlayer distance (0.335 nm) [47] in regular graphite. Then, nanographite domains are weakly linked with each other in a random fashion, giving the 3D disordered network. Accordingly, this hierarchical loose structure of ACFs offers a mechanically flexible micropore network which can accommodate a large amount of various guest molecules [75]. In other words, the 3D network of nanographene sheets connected to each other through two kinds of soft springs is susceptible to an external mechanical perturbation if the internanographene sheet interaction within a nanographite domain and the internanographite interaction are the two kinds of springs. The combination of micropores with nanographenes, in the edges of which localized magnetic moments of the edge states exist, allows us to utilize the edge-state spins in detecting guest molecules adsorbed in the micropores, taking into account that the adsorption of molecules gives a mechanical perturbation to the flexible micropores. In this section, two useful applications of the edge-state spins in adsorption of molecules are discussed in microporous ACFs.

A. Molecule sensor

Figure 16 shows the adsorption isotherm of H_2O molecules and the accompanying change in the magnetic susceptibility in ACFs at room temperature [44]. H_2O

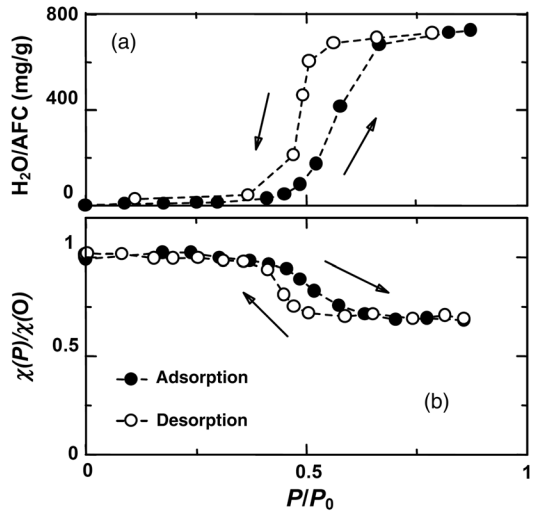

FIG. 16. (a) The H_2O adsorption isotherm and (b) the spin susceptibility χ_s as a function of vapor pressure P of H_2O at room temperature. P_0 is the saturation vapor pressure. (After Ref. [44].)

molecules are hardly adsorbed in the micropores in the low vapor-pressure range and start to be adsorbed in a discontinuous manner at a threshold vapor pressure of $P_t/P_0 \sim 0.5$. Then, the adsorption is saturated just after the threshold vapor pressure. The desorption of H_2O molecules is reversible to the adsorption, except for the presence of a hysteresis between the adsorption and desorption processes at the threshold vapor pressure. Interestingly, x-ray diffraction experiments indicate a large reduction in the internanographene sheet distance from 0.38 to 0.34 nm at P_t, suggesting that the H_2O adsorption taking place above the threshold vapor pressure squeezes the loosely packed nanographite domain in order to allow the micropore space to be expanded for the adsorbed H_2O molecules [44]. Namely, the adsorbed H_2O molecules work as a mechanical force, resulting in the squeeze. This stepwise reversible adsorption or desorption isotherm accompanied with the reduction or restoration in the internanographene sheet distance is related to the hydrophobicity of nanographene surfaces. A repulsive force acting between the hydrophobic nanographene surfaces and adsorbed H_2O molecules works to squeeze the nanographite domains above P_t, taking into account that the micropores are surrounded by nanographite domains in all directions [see Fig. 7(a)].

The magnetic susceptibility, which represents the net magnetic moment of the ferrimagnetic (superparamagnetic) structure of an individual nanographene sheet, shows a sharp discontinuous drop at the threshold vapor pressure by 30%–40% with a hysteresis between the adsorption and desorption processes. According to theoretical calculation [76], the antiferromagnetic exchange interaction $J_{2,\text{intradomain}}$ between the magnetic moments of the adjacent nanographene sheets within a nanographite domain is negligible at room temperature for the elongated internanographene sheet distance of 0.38 nm due to the absence of wave-function overlap between nanographene sheets. Consequently, the ferrimagnetic moment in a nanographene sheet behaves independently from that in the adjacent nanographene sheet. However, when the internanographene sheet distance reduces to 0.34 nm, which is close to the interlayer distance in regular graphite [47], upon H_2O adsorption, the wave-function overlap cannot be negligible, and the enhancement of $J_{2,\text{intradomain}}$ works to arrange the ferrimagnetic moments antiparallel to each other, resulting in a decrease in the net magnetic moment of the nanographite domain as schematically shown in Fig. 17.

This reversible on-off type magnetic switching behavior at a threshold vapor pressure is observed also in the adsorption of other molecules having OH groups such as CH_3OH and C_2H_5OH as shown in Fig. 18 [45,58]. However, the behavior becomes less clear in addition to the threshold vapor pressure shifting down in these OH-containing molecules. In sharp contrast to the OH-containing molecules, adsorption takes place from the low-vapor-pressure range with no finite threshold vapor pressure, and the magnetic switching phenomena are not observed for OH-absent molecules such as $(CH_3)_2CO$, C_6H_6, $CHCl_3$, CCl_4, C_6H_{12}, C_6H_{14}, as evidenced in Fig. 18. These findings demonstrate that the repulsive force acting between the hydrophobic nanographene surface and the OH-containing molecules weakens upon the decrease in the weight of OH group, ensuing the lowering of the threshold vapor pressure P_t: $H_2O > CH_3OH, C_2H_5OH$. In the OH-absent molecules, which interact with nanographene with attractive force, molecular adsorption takes place easily with no threshold vapor pressure, resulting in the absence of magnetic switching phenomena.

The experimental results in which the presence or absence of the on-off magnetic switching phenomenon depending on the contribution of the OH groups in the molecule adsorption allow us to utilize the edge-state spins as a detection probe for a molecule sensor based on nanographene-based microporous ACFs.

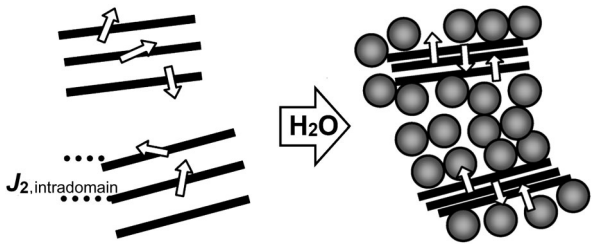

FIG. 17. Magnetic switching phenomenon. $J_{2,\text{intradomain}}$ is the inter-nanographene-sheet antiferromagnetic interaction in a nanographite domain. The compression of nanographite domains by H_2O molecules (shaded circle) condensed in the nanopores strengthens $J_{2,\text{intradomain}}$. The arrow indicates the net magnetic moment in an individual nanographene sheet.

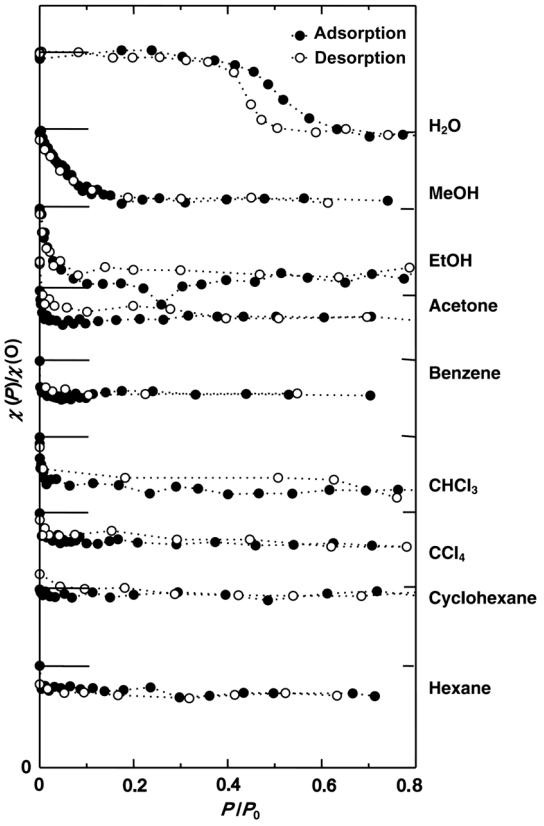

FIG. 18. The spin susceptibilities of ACFs under the vapor pressure P of various guest molecules: H_2O, CH_3OH, C_2H_5OH, $(CH_3)_2CO$, C_6H_6, $CHCl_3$, CCl_4, C_6H_{12}, C_6H_{14} at room temperature. P_0 is the saturation vapor pressure at room temperature. The vertical axis is shifted for each plot for clarity, where the distance between the bars is 0.3 except for the top and bottom plots. (After Ref. [45].)

B. Helium detector

Molecule adsorption crucially depends on the size of the molecules accommodated in the micropores of ACFs. Figure 19 shows the adsorption isotherms for N_2, O_2, He, and Ar in the micropores of ACFs at room temperature [46,77]. The effective pressure of guest molecules inside the micropores is orders of magnitude larger than the pressure of the molecules in the gaseous state in the environment. Actually, around a gaseous pressure of 100 Torr, the effective pressure inside the micropores goes to 7–10 atm for N_2, Ar, and O_2. This means there is a large condensation of guest molecule species in the micropores owing to the enhanced condensation energy associated with molecule-nanographene interaction of the molecules confined in a narrow micropore space [73,74]. An exceptionally huge condensation takes place in the case of He; that is, the pressure inside reaches almost 80 atm, which corresponds to about one-tenth of the density of liquid helium, even when the vapor pressure of He is 10 Torr. Here, the condensation rate is over 6000 indeed.

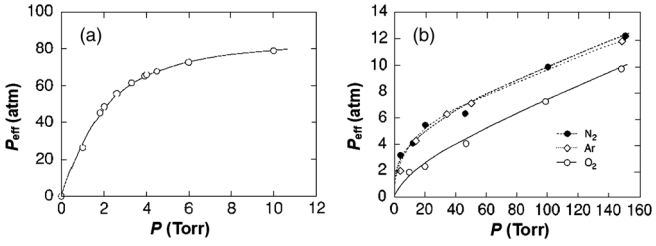

FIG. 19. Effective pressure for (a) He, (b) N_2, O_2, and Ar in the micropores of ACFs at room temperature as a function of the external pressure. (After Ref. [46].)

The molecule adsorption phenomenon in the micropores that is investigated using molecule adsorption isotherms can be tracked by ESR of the edge-state spins. Here, the ESR saturation technique gives information on the spin-lattice relaxation process of the edge-state spins in nanographenes. The energy that the spin system gains from the microwave is relaxed to the environment through the spin-lattice relaxation process, which is mediated by phonons in general. Figure 20 presents the microwave power dependence of the ESR intensity (saturation curve) taken at room temperature in vacuum and in the atmosphere of 10 Torr He, O_2, Ar, and N_2. In vacuum, the ESR signal tends to be easily saturated in the low microwave power range, suggesting that the energy flow from the edge-state spins to the environment is considerably slow due to the small spin-lattice relaxation rate $1/T_1$. The relaxation is driven by the acoustic phonons, whose Debye temperature is considerably high in the range of 2000 K for bulk graphite [47]. When the size of the graphite is reduced, the phonon energy becomes discrete due to the quantum-size effect. Indeed, in the case of nanographene having an in-plane size of 2 nm, the discreteness of phonons reaches approximately 200 K, making the contribution of the phonons less effective especially at low temperatures. This quantum-size effect of phonons is the reason why the relaxation rate in the edge-sate spins becomes small in nanographene. Meanwhile, the

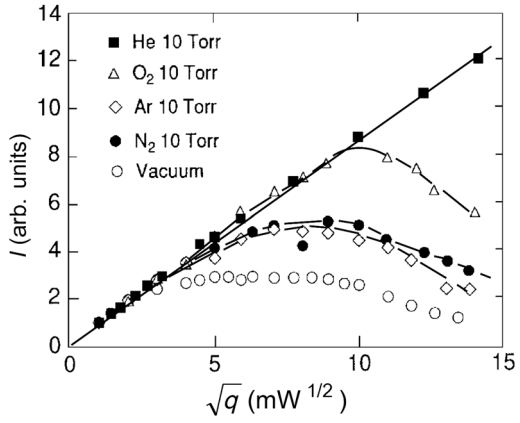

FIG. 20. ESR saturation curves for 10 Torr of He, O_2, Ar, and N_2 in ACFs at room temperature. The saturation curve in vacuum is also shown. (After Ref. [46].)

introduction of gaseous molecule species revives the spin-lattice relaxation path, giving a less saturated feature in the saturation curves in the atmosphere of gaseous molecules, as shown in Fig. 20. The extreme case occurs in the He atmosphere, where no saturation appears in the microwave power range investigated. In other words, the energy absorbed in the edge-state spins from the microwave can be easily relaxed to the environment in the atmosphere of He. These experimental findings strongly suggest an important contribution of guest gaseous molecules to the spin-lattice relaxation mechanism.

In the micropores, guest molecules collide with edge-state spin sites around the peripheries of a nanographene sheet. The collisional process, which is governed by van der Waals interaction between a guest molecule and nanographene, works effectively to accelerate the spin-lattice relaxation rate, particularly for the case in which the phonon-assisted process is not at work if it is incorporated with the spin-reversal event [78]. In this case, relaxation rate $1/T_1$ in the collision-induced relaxation process is described in the following equation,

$$1/T_1 = nv\sigma, \tag{6}$$

where n and σ are the density of guest molecules and the cross section related to the spin-flip process, respectively. v is the mean velocity of the molecules,

$$v = \sqrt{3RT/M}, \tag{7}$$

where M is the mass of the guest molecule. A more detailed analytical expression can be obtained on the basis of the electric dipole-dipole interaction between a molecule and nanographene, which is given for the He molecule as follows:

$$1/T_1 = \left[\frac{6.05}{9(2\pi)^{1/2}\hbar^4}\right] nM^{3/2}\left(\frac{p}{\Delta E}\right)^2\left[\frac{(e^2IJ)^4}{{R_0}^6}\right] w(k_BT)^{1/2}, \tag{8}$$

where R_0 is the minimum distance in which a He molecule can access an edge-spin site. I, J, and ΔE are parameters related to the electronic structure of the He molecule. p is given to be λ/Δ, where λ is the spin-orbit interaction of the carbon p state (approximately 5 cm^{-1}) [68], and Δ is the energy difference between the excited and ground states of edge-state spins. w is the probability of the carbon $2p_z$ state being vacant. Equation (8) well reproduces the experimental results, suggesting that the edge-state spins work as a probe of He molecules.

An important issue that should be pointed out is the exceptionally large He condensation in the ACF micropores. It is related to the presence of ultramicropores [79], to which only a smallest diameter He atom (0.257 nm) can access. This finding allows us to utilize the edge-state spin as a probe in a He detector on the basis of nanographene-based microporous carbon.

VI. SUMMARY

Nanographenes, which are created by cutting a graphene sheet into nanodimension or considered as nanosized polycyclic aromatic hydrocarbon molecules, have important edge geometry dependence in their electronic structures. In armchair edges, electron wave interference works to create a standing wave, which contributes to aromatic (energetic) stability. Accordingly, semiconductive armchair-edged nanographenes with an open energy gap are interesting nanocarbon materials for electronic device applications such as field-effect transistors. Meanwhile, zigzag edges possess an edge-localized and spin-polarized nonbonding π-electron state (edge state), which causes electronic, magnetic, and chemical activities. Particularly, the edge-state spins localized in zigzag edges are an intriguing target in molecular magnetism and also device applications such as spintronic devices and magnetic probes. The edge-geometry-dependent electronic structures are discussed comprehensively by approaching them from both bottom-up chemistry and top-down physics bases. In addition, applications of the edge-state spins as a probe in molecule adsorption in nanographene-based microporous carbon are proposed.

A nanographene sheet has a periphery consisting of a combination of nonmagnetic armchair and magnetic zigzag edges. The interplay of strong ferromagnetic intra-zigzag-edge interaction and intermediate-strength ferromagnetic or antiferromagnetic inter-zigzag-edge interaction gives a ferrimagnetic structure with a nonzero net magnetic moment, whose strength depends on their size and shape.

The electronic and magnetic structures, which primarily depend on the edge geometry, also vary depending on how the edge carbon atoms are terminated with foreign chemical species. The variation induced by this edge chemistry detail can be tracked experimentally by high-temperature annealing of nanographene sheets. In nanographene sheets handled in ambient atmosphere, the edges are terminated mostly with oxygen-containing functional groups. Here, the zigzag edges terminated with the oxygen-containing functional group have less localized edge state due to the charge transfer from nanographene to electronegative oxygen atoms. This charge transfer effect results in stabilizing nonbonding edge states, which are otherwise unstable and chemically reactive. The survival of an edge state in nanographene handled in ambient atmospheric conditions is due to this rather stable feature of zigzag edges terminated with oxygen-containing functional groups. Oxygen-containing functional groups are decomposed and removed from the edges in high-temperature heat treatment, and, instead, hydrogen becomes the majority in the edge-terminating groups around 1500 K, at which fusion starts if the nanographene sheets are close to each

other. Hydrogen-terminated zigzag edges have an unstable edge state well localized in the vicinity of the edges. The removal of hydrogen at chemically active zigzag edges triggers fusion. The percolative development of local fusion brings about an *I*-*M* transition in the disordered network of nanographene sheets. It induces short-range antiferromagnetic ordering in the disordered network of ferrimagnetic nanographenes, resulting in the formation of a spin-glass state around the *I*-*M* transition.

For applications, the edge-state spins can be utilized as a probe in molecule sensors in molecule adsorption into nanographene-based microporous carbon. The hydrophobicity of the nanographene surface works to distinguish molecules adsorbed in the micropores depending on the presence or absence of OH groups in the molecules. Namely, a repulsive force works between the nanographene surface and OH-containing molecules, whereas an attractive force is present in OH-absent molecules. The repulsive force created in the adsorption of OH-containing molecules brings about a reversible contraction or restoration of nanographite domains with a threshold vapor pressure, resulting in an on-off-type switching in the magnetic moments of nanographenes. This magnetic switching phenomenon upon adsorption of OH-containing molecules offers a useful application of the edge-state spin for a molecular sensor. The molecule size dependence in molecule adsorption is particularly important in the case of He molecules accommodated in ultramicropores, to which only the smallest diameter He molecules can access. The He atoms confined to ultramicropores participate in a collision-induced heat-transfer process from the edge-state spins, giving a drastic change in the spin dynamics. A He sensor can be proposed in which the edge-state spins are utilized as a probe.

A variety of electronic, magnetic, and chemical properties of nanographene offers important insight into understanding the functionalities of graphitic carbon materials. Importantly, the present work on the edge chemistry details of nanographenes in ambient atmospheric conditions and their dependence on high-temperature annealing gives the answer to the long-lasting question on what the actual graphene edges are. It also offers valuable information for the handling of nanographenes in creating nanographene-based electronic or spintronic device applications. Moreover, the applications of the edge-state spins as a probe in a molecule sensor are practically important.

ACKNOWLEDGMENTS

We would like to acknowledge J. Takashiro, V. L. Joseph Joly, M. Ziatdinov, M. Otsuka, K. Takahara, N. Kawatsu, Y. Shibayama, A. Nakayama, S. Fujii, K. Takai and H. Sato for their contributions to the work related to the present article. We would like to express our thanks to K. Kusakabe, T. Mori, M. Endo. K. Kaneko, T. Kyotani, K. Sugihara, and P. Eklund for their fruitful discussions. We extend our deepest appreciation to M. S. Dresselhaus for her continuous encouragement and fruitful discussion from the early stage of our work to the present. In particular, what she has inspired in us allowed us to gain comprehensive understanding of the magnetism of graphitic carbon as summarized in this article.

[1] E. Clar, *The Aromatic Sextet* (Wiley, London, 1972).
[2] K. Sasaki and R. Saito, Pseudospin and deformation-induced gauge field in graphene, Prog. Theor. Phys. Suppl. **176**, 253 (2008).
[3] A. H. Castro Neto, F. Guinea, N. M. Peres, K. S. Novoselov, and A. K. Geim, The electronic properties of graphene, Rev. Mod. Phys. **81**, 109 (2009).
[4] T. Enoki and T. Ando, *Physics and Chemistry of Graphene, Graphene to Nanographene* (Pan Stanford Publishing, Singapore, 2013).
[5] T. Enoki, Y. Kobayashi, and K. Fukui, Electronic structures of graphene edges and nanographene, Int. Rev. Phys. Chem. **26**, 609 (2007).
[6] S. Fujii and T. Enoki, Nanographene and graphene edges: Electronic structure and nanofabrication, Acc. Chem. Res. **46**, 2202 (2013).
[7] S. Fujii, M. Ziatdinov, M. Ohtsuka, K. Kusakabe, M. Kiguchi, and T. Enoki, Role of edge geometry and chemistry in the electronic properties of graphene nanostructures, Faraday Discuss. Chem. Soc. **173**, 173 (2014).
[8] K. Müllen and J. P. Rabe, Nanographenes as active components of single-molecule electronics and how a scanning tunneling microscope puts them to work, Acc. Chem. Res. **41**, 511 (2008).
[9] P. Ruffieux, S. Wang, B. Yang, C. Sánchez-Sánchez, J. Liu, T. Dienel, L. Talirz, P. Shinde, C. A. Pignedoli, D. Passerone, T. Dumslaff, X. Feng, K. Müllen, and R. Fasel, On-surface synthesis of graphene nanoribbons with zigzag edge topology, Nature (London) **531**, 489 (2016).
[10] Y.-C. Chen, T. Cao, Z. Chen, C. Pedramrazi, D. Haberer, D. G. de Oteyza, F. R. Fischer, S. G. Louie, and M. Crommie, Molecular bandgap engineering of bottom-up synthesized graphene nanoribbon heterojunctions, Nat. Nanotechnol. **10**, 156 (2015).
[11] T. Wassmann, A. P. Seitsonen, A. Marco Saitta, M. Lazzeri, and F. Mauri, Clar's theory, π-electron distribution, and geometry of graphene nanoribbons, J. Am. Chem. Soc. **132**, 3440 (2010).
[12] K. Ozaki, K. Kawasumi, M. Shibata, H. Ito, and K. Itami, One-shot *K*-region-selective annulative π-extension for nanographene synthesis and functionalization, Nat. Commun. **6**, 6251 (2015).
[13] L. Yang, C.-H. Park, Y.-W. Son, M. L. Cohen, and S. G. Louie, Quasiparticle Energies and Band Gaps in Graphene Nanoribbons, Phys. Rev. Lett. **99**, 186801 (2007).
[14] Q. Yan, B. Huang, J. Yu, F. Zheng, J. Zang, J. Wu, B.-L. Gu, F. Liu, and W. Duan, Intrinsic current-voltage characteristics of graphene nanoribbon transistors and effect of edge doping, Nano Lett. **7**, 1469 (2007).

[15] M. Maruyama and K. Kusakabe, Theoretical prediction of synthesis methods to create magnetic nanographite, J. Phys. Soc. Jpn. **73**, 656 (2004).
[16] J. Fernández-Rossier and J. J. Palacios, Magnetism in Graphene Nanoislands, Phys. Rev. Lett. **99**, 177204 (2007).
[17] O. V. Yazyev and M. I. Katsnelson, Magnetic Correlations at Graphene Edges: Basis for Novel Spintronics Devices, Phys. Rev. Lett. **100**, 047209 (2008).
[18] T. Enoki and K. Takai, The edge state of nanographene and the magnetism of the edge-state spins, Solid State Commun. **149**, 1144 (2009).
[19] P. Esquinazi, R. Höhne, K.-H. Han, D. Spemann, A. Setzer, M. Diaconu, K. Schmidt, and T. Butz, in *Carbon Based Magnetism: An Overview of the Magnetism of Metal Free Carbon-based Compounds and Materials*, edited by T. L. Makarova and F. Palacio (Elsevier, Amsterdam, 2006), p. 437.
[20] S. S. Gregersen, S. R. Power, and A.-P. Jauho, Nanostructured graphene for spintronics, Phys. Rev. B **95**, 121406 (2017).
[21] Z.-Q. Fan, W.-Y. Sun, Z.-H. Zhang, X.-Q. Deng, G.-P. Tang, and H.-Q. Xie, Symmetry-dependent spin transport properties of a single phenalenyl or pyrene molecular device, Carbon **122**, 687 (2017).
[22] T. Wassmann, A. P. Seitsonen, A. M. Saitta, M. Lazzeri, and F. Mauri, Structure, Stability, Edge States, and Aromaticity of Graphene Ribbons, Phys. Rev. Lett. **101**, 096402 (2008).
[23] O. Hod, V. Barone, J. E. Peralta, and G. E. Scuseria, Enhanced half-metallicity in edge-oxidized zigzag graphene nanoribbons, Nano Lett. **7**, 2295 (2007).
[24] D. E. Jiang, B. G. Sumpter, and S. Dai, Unique chemical reactivity of a graphene nanoribbon's zigzag edge, J. Chem. Phys. **126**, 134701 (2007).
[25] M. Ziatdinov, H. Lim, S. Fujii, K. Kusakabe, M. Kiguchi, T. Enoki, and Y. Kim, Chemically induced topological zero mode at graphene armchair edges, Phys. Chem. Chem. Phys. **19**, 5145 (2017).
[26] Q. Gao and J. Guo, Role of chemical termination in edge contact to graphene, APL Mater. **2**, 056105 (2014).
[27] A. Bellunato, H. A. Tash, Y. Cesa, and G. F. Schneider, Chemistry at the edge of graphene, ChemPhysChem **17**, 785 (2016).
[28] S. Mrozowski, Semiconductivity and diamagnetism of polycrystalline graphite and condensed ring systems, Phys. Rev. **85**, 609 (1952).
[29] J. M. Thomas, in *Chemistry and Physics of Carbon*, edited by P. L. Walker, Jr. (Marcel Dekker, New York, 1965), Vol. 1, p. 121.
[30] M. Inagaki and L. R. Radovic, Nanocarbons, Carbon **40**, 2279 (2002).
[31] H. Aso, K. Matsuoka, A. Sharma, and A. Tomita, Evaluation of size of graphene sheet in anthracite by a temperature-programmed oxidation method, Energy Fuels **18**, 1309 (2004).
[32] L. R. Radovic and B. Bockrath, On the chemical nature of graphene edges: Origin of stability and potential for magnetism in carbon materials, J. Am. Chem. Soc. **127**, 5917 (2005).
[33] G. U. Sumanasekera, G. Chen, K. Takai, J. Joly, N. Kobayashi, T. Enoki, and P. C. Eklund, Charge transfer and weak chemisorption of oxygen molecules in nanoporous carbon consisting of a disordered network of nanographene sheets, J. Phys. Condens. Matter **22**, 334208 (2010).
[34] D. W. Boukhvalov, V. Yu. Osipov, A. I. Shames, K. Takai, T. Hayashi, and T. Enoki, Charge transfer and weak bonding between molecular oxygen and graphene zigzag edges at low temperatures, Carbon **107**, 800 (2016).
[35] Y. Shibayama, H. Sato, T. Enoki, X. Xin Bi, M. S. Dresselhaus, and M. Endo, Novel electronic properties of a nano-graphite disordered network and their iodine doping effects, J. Phys. Soc. Jpn. **69**, 754 (2000).
[36] Y. Shibayama, H. Sato, T. Enoki, and M. Endo, Disordered Magnetism at the Metal-Insulator Threshold in Nano-Graphite-Based Carbon Materials, Phys. Rev. Lett. **84**, 1744 (2000).
[37] V. L. Joseph Joly, K. Takahara, K. Takai, K. Sugihara, T. Enoki, M. Koshino, and H. Tanaka, Phys. Rev. B **81**, 115408 (2010).
[38] V. L. Joseph Joly, M. Kiguchi, K. Takai, T. Enoki, R. Sumii, K. Amemiya, H. Muramatsu, T. Hayashi, Y. A. Kim, M. Endo, M. Terrones, and M. S. Dresselhaus, Observation of magnetic edge state in graphene nanoribbons, Phys. Rev. B **81**, 245428 (2010).
[39] M. Kiguchi, K. Takai, V. L. Joseph Joly, T. Enoki, R. Sumii, and K. Amemiya, Magnetic edge state and dangling bond state of nanographene in activated carbon fibers, Phys. Rev. B **84**, 045421 (2011).
[40] J. Takashiro, Y. Kudo, S. Kaneko, K. Takai, T. Ishii, T. Kyotani, T. Enoki, and M. Kiguchi, Heat treatment effect on the electronic and magnetic structures of nanographene sheets investigated through electron spectroscopy and conductance measurements, Phys. Chem. Chem. Phys. **16**, 7280 (2014).
[41] M. Ziatdinov, S. Fujii, K. Kusakabe, M. Kiguchi, T. Mori, and T. Enoki, Visualization of electronic states on atomically smooth graphitic edges with different types of hydrogen termination, Phys. Rev. B **87**, 115427 (2013).
[42] M. Otshuka, S. Fujii, M. Kiguchi, and T. Enoki, Electronic state of oxidized nanographene edge with atomically sharp zigzag boundaries, ACS Nano **7**, 6868 (2013).
[43] M. Ziatdinov, S. Fujii, K. Kusakabe, M. Kiguchi, T. Mori1, and T. Enoki, Direct imaging of monovacancy-hydrogen complexes in a single graphitic layer, Phys. Rev. B **89**, 155405 (2014).
[44] H. Sato, N. Kawatsu, T. Enoki, M. Endo, R. Kobori, S. Maruyama, and K. Kaneko, Drastic effect of water-adsorption on the magnetism of carbon nanomagnets, Solid State Commun. **125**, 641 (2003).
[45] H. Sato, N. Kawatsu, T. Enoki, M. Endo, R. Kobori, S. Maruyama, and K. Kaneko, Physisorption-induced change in the magnetism of microporous carbon, Carbon **45**, 214 (2007).
[46] A. Nakayama, K. Suzuki, T. Enoki, C. Ishii, K. Kaneko, M. Endo, and N. Shindo, Anomalous helium-gas-induced spin-lattice relaxation and the evidence for ultra micropores in microporous carbon, Solid State Commun. **93**, 323 (1995).
[47] B. T. Kelly, *Physics of Graphite* (Applied Science Publishers, London, 1981).

[48] J. R. Schaibley, H. Yu, G. Clark, P. Rivera, J. S. Ross, K. L. Seyler, W. Yao, and X. Xu, Valleytronics in 2D materials, Nat. Rev. Mater. **1**, 16055 (2016).
[49] K. Tanaka, S. Yamashita, H. Yamabe, and T. Yamabe, Electronic properties of one-dimensional graphite family, Synth. Met. **17**, 143 (1987).
[50] S. E. Stein and R. L. Brown, π-electron properties of large condensed polyaromatic hydrocarbons, J. Am. Chem. Soc. **109**, 3721 (1987).
[51] D. J. Klein, Graphitic polymer strips with edge state, Chem. Phys. Lett. **217**, 261 (1994).
[52] M. Fujita, K. Wakabayashi, K. Nakada, and K. Kusakabe, Peculiar localized state at zigzag graphite edge, J. Phys. Soc. Jpn. **65**, 1920 (1996).
[53] K. Nakada, M. Fujita, G. Dresselhaus, and M. S. Dresselhaus, Edge state in graphene ribbons: Nanometer size effect and edge shape dependence, Phys. Rev. B **54**, 17954 (1996).
[54] M. Bendikov, H. M. Duong, K. Starkey, K. N. Houk, E. A. Carter, and F. Wudl, Oligoacenes: Theoretical prediction of open-shell singlet diradical ground states, J. Am. Chem. Soc. **126**, 7416 (2004).
[55] M. S. Dresselhaus, A. W. P. Fung, A. M. Rao, S. L. di Vittorio, K. Kuriyama, and M. Endo, New characterization techniques for activated carbon fibers, Carbon **30**, 1065 (1992).
[56] A. Nakayama, K. Suzuki, T. Enoki, K. Koga, M. Endo, and N. Shindo, Electronic and magnetic properties of activated carbon fibers, Bull. Chem. Soc. Jpn. **69**, 333 (1996).
[57] T. Enoki, Role of edges in the electronic and magnetic structures of nanographene, Phys. Scr. **T146**, 014008 (2012).
[58] T. Enoki, K. Takai, and M. Kiguchi, Magnetic edge state of nanographene and unconventional nanographene-based host-guest systems, Bull. Chem. Soc. Jpn. **85**, 249 (2012).
[59] K. Wakabayashi, M. Sigrist, and M. Fujita, Spin wave mode of edge-localized magnetic states in nanographite zigzag ribbons, J. Phys. Soc. Jpn. **67**, 2089 (1998).
[60] J. Fernández-Rossier and J. J. Palacios, Magnetism in Graphene Nanoislands, Phys. Rev. Lett. **99**, 177204 (2007).
[61] B. Ranby and J. F. Rabek, *ESR Spectroscopy in Polymer Research, Polymers/Properties and Applications I* (Springer-Verlag, Berlin, 1977).
[62] A. W. P. Fung, Z. H. Wang, M. S. Dresselhaus, G. Dresselhaus, R. W. Pekala, and M. Endo, Coulomb-gap magnetotransport in granular and porous carbon structures, Phys. Rev. B **49**, 17325 (1994).
[63] A. L. Efros and B. I. Shklovskii, Coulomb gap and low temperature conductivity of disordered systems, J. Phys. C **8**, L49 (1975).
[64] A. Aharony and A. B. Harris, Superlocalization, correlations and random walks on fractals, Physica (Amsterdam) **163A**, 38 (1990).
[65] A. Aharony, O. Entin-Wohlman, and A. B. Harris, Was superlocalization observed on a fractal?, Physica (Amsterdam) **200A**, 171 (1993).
[66] J. Korringa, Nuclear magnetic relaxation and resonance line shift in metals, Physica (Utrecht) **16**, 601 (1950).
[67] H. Hasegawa, Dynamical properties of *s-d* interaction, Prog. Theor. Phys. **21**, 483 (1959).
[68] K. Matsubara, T. Tsuzuku, and K. Sugihara, Electron spin resonance in graphite, Phys. Rev. B **44**, 11845 (1991).
[69] T. L. Makarova and F. Palacio, *Carbon-Based Magnetism* (Elsevier, Amsterdam, 2006).
[70] N. Kobayashi, T. Enoki, C. Ishii, K. Kaneko, and M. Endo, Gas adsorption effects on structural and electrical properties of activated carbon fibers, J. Chem. Phys. **109**, 1983 (1998).
[71] J. Takashiro, Y. Kudo, S-J. Hao, K. Takai, D. N. Futaba, T. Enoki, and M. Kiguchi, Preferential oxidation-induced etching of zigzag edges in nanographene, Phys. Chem. Chem. Phys. **16**, 21363 (2014).
[72] Z. Hou, X. Wang, T. Ikeda, S.-F. Huang, K. Terakura, M. Boero, M. Oshima, M. Kakimoto, and S. Miyata, Effect of hydrogen termination on carbon *K*-edge x-ray absorption spectra of nanographene, J. Phys. Chem. C **115**, 5392 (2011).
[73] M. Thommes, K. Kaneko, A. V. Neimark, J. P. Olivier, F. Rodriguez-Reinoso, J. Rouquerol, and K. S. W. Sing, Physisorption of gases, with special reference to the evaluation of surface area and pore size distribution (IUPAC Technical Report), Pure Appl. Chem. **87**, 1051 (2015).
[74] S. Wang, D. Ábrahám, F. Vallejos-Burgos, K. László, E. Geissler, K. Takeuchi, M. Endo, and K. Kaneko, Distorted graphene sheet structure-derived latent nanoporosity, Langmuir **32**, 5617 (2016).
[75] T. Suzuki and K. Kaneko, Structural change of activated carbon fibers with desorption by *in situ* x-ray diffraction, Carbon **26**, 743 (1988).
[76] K. Harigaya and T. Enoki, Mechanism of magnetism in stacked nanographite with open shell electrons, Chem. Phys. Lett. **351**, 128 (2002).
[77] K. Takahara, S. Hao, H. Tanaka, T. Kadono, M. Hara, K. Takai, and T. Enoki, Mechanical compression induced short-range ordering of nanographene spins, Phys. Rev. B **82**, 121417 (2010).
[78] K. Sugihara, A. Nakayama, and T. Enoki, Anomalous spin-lattice relaxation induced by helium gas in microporous carbon, J. Phys. Soc. Jpn. **64**, 2614 (1995).
[79] K. Kaneko, Determination of pore size and pore size distribution: 1. Adsorbents and catalysts, J. Membr. Sci. **96**, 59 (1994).